Using Faraday Waves to Measure Interfacial Tension

Lau, Yuk Man; Westerweel, Jerry; van de Water, Willem

DOI
10.1021/acs.langmuir.0c00622

Publication date
2020

Document Version
Final published version

Published in
Langmuir : the ACS journal of surfaces and colloids

LANGMUIR

pubs.acs.org/Langmuir Article

Using Faraday Waves to Measure Interfacial Tension

Yuk Man Lau, Jerry Westerweel, and Willem van de Water*

Cite This: *Langmuir* 2020, 36, 5872−5879

Read Online

ACCESS | Metrics & More | Article Recommendations

ABSTRACT: We use Faraday waves to measure interfacial tension σ between two immiscible fluids, with an interest in (ultra)low values of σ. The waves are excited by vertically oscillating the container in which the fluids reside. Using linear stability theory, we map out the accessible range of interfacial tensions. The smallest value ($\sigma_{min} \approx 5 \times 10^{-4}$ N/m) is limited by the joint influence of gravity and viscous dissipation. A further limitation is posed by the greatest accelerations that can be realized in a laboratory. We perform experiments on a water−dodecane interface with an increasing concentration of a surfactant in the water layer that decreases the interfacial tension into the ultralow domain [$\sigma = O(10^{-6}$ N/m)]. Surprisingly, the smallest measured wavelength is larger by a factor of 2 than that predicted for vanishing σ. We hypothesize the effect of transport of the surfactant in the fluid flow associated with the waves.

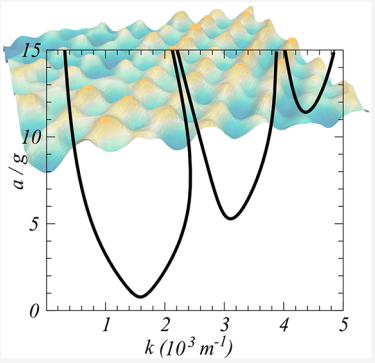

INTRODUCTION

It is a challenge to measure ultralow interface tensions between two fluids [$\sigma = O(10^{-6}$ N/m)]. A standard method used to measure interfacial tensions is the pendant drop method in which the shape of a drop of immiscible heavier fluid 1 inside lighter fluid 2 depends on the mass densities $\rho_1 > \rho_2$ and on the interfacial tension.[1] When the interfacial tension is small, the performance of the experiment is delicate. Smaller interfacial tensions ($\sigma \gtrsim 10^{-6}$ N/m) can be reached via the spinning drop method.[2,3] There, the shape of the drop is determined by the balance between inertial (centrifugal) forces and interface tension. It is a static technique in which the interface remains stationary in the rotating frame. With a decrease in interfacial tension, the relaxation of the interface becomes increasingly slow.

As rapid measurements of interfacial tension may help in the design of fluids for chemically enhanced oil recovery, several designs for microfluidic tensiometers have been reported.[4,5] An interesting recent paper infers the interfacial tension from the phase diagram of pattern formation of immiscible co-flowing fluids.[6] Then, the challenge is to parametrize the phase diagram, including its dependence on other fluid parameters, such as viscosity and density. In this experiment, the lowest σ detected was $\approx 10^{-5}$ N/m.

In this paper, we will explore waves on the interface between water and dodecane to determine the interfacial tension. These waves are excited mechanically, by vertically oscillating the container in which the two fluids are placed. The waves arise through a parametric instability and are known as Faraday waves. The linear stability theory by Kumar and Tuckerman,[7] which is applied in this paper, makes use of the periodic nature of the excitation and involves linearized boundary conditions on the interface and on the top and bottom surfaces. Waves offer the tantalizing prospect of a measuring device for interfacial tension: they are driven through oscillation, and their wavelength, telltale of σ, can simply be measured from an image.

A completely different range of wavelengths can be probed by observing the thermal fluctuations of the interface.[4,8−10] This can be done by scattering (coherent) light,[8] where the thermal wavelength follows from the scattering angle, or directly in real space by microscopic observation.[9] Very small interfacial tensions $\sigma = O(10^{-7})$ N/m can be observed in this way.[4,9,10] However, the amplitude of the interfacial waves (or the intensity of scattered light) rapidly decreases with an increase in interfacial tension, so that only ultralow interfacial tensions are accessible with this method.

Waves on a fluid with an insoluble surfactant layer were discussed in a seminal paper by Lucassen-Reynders and Lucassen.[11] Their viscoelastic properties can be inferred from a measurement of the wavelength and damping.[12] The relation between wave height and the dynamics of an insoluble surfactant layer was measured by Strickland et al.[13] Faraday waves on the liquid−vapor interface of CO_2 near the critical point were observed by Fauve et al.[14] Much as in this paper they also found saturation of the wavelength at vanishing σ and emphasize the importance of viscous dissipation. The other

Received: March 4, 2020
Revised: April 20, 2020
Published: April 22, 2020

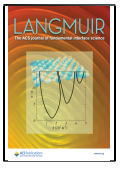

https://dx.doi.org/10.1021/acs.langmuir.0c00622
Langmuir 2020, 36, 5872−5879

extreme is formed by Faraday waves on an unextensible surface layer arising in a freezing transition.[15]

The behavior of a soluble surfactant in a dynamic experiment, such as that presented here, is extremely complex. Its local concentration is governed by fluid motion, which, in turn, is influenced by the resulting interfacial tension. There is a strong two-way coupling in this problem, even to the point that the notion of "interfacial tension" may become ambiguous.

Gradients of surfactant concentration induced by fluid flow or diffusion lead to gradients of interfacial tension: Marangoni stresses. It has been suggested that these stresses increase the onset the driving amplitude of Faraday waves and influence the onset wavenumber.[16] A theoretical study was performed by Kumar and Matar,[17] using Floquet techniques similar to those applied to the two-layer case.[7] Surprisingly, only a small effect was found on the onset amplitude, and an even smaller effect on the onset wavenumber. In their approach, a linear stability analysis, the equation of surfactant transport was linearized, with the concentration along the surface assumed to be constant. This restriction was overcome in a treatment of thin liquid layers.[18−20]

The concentration Γ_{int} of the surfactant at the interface determines the interfacial tension σ through the equation of state. As adhesion and desorption of surfactant molecules at the interface play a key role, Γ_{int} is not the same as the bulk concentration Γ taken at the interface. These absorption and desorption rates are not known very well. All of these phenomena were considered in a novel numerical method for three-dimensional multiphase flows that was recently published by Shin et al.[21] Two-dimensional Faraday waves covered by an insoluble surfactant were investigated numerically by Ubal et al.[22]

In our experiments, we dissolve a surfactant at increasing concentrations in the water layer, and we infer the interfacial tension σ between water and dodecane from the measured wavelengths of Faraday waves. As a consistency check, we predict the onset excitation amplitude from σ and compare it to the experimental one. In the next section, we will present model calculations of linear Floquet theory by Kumar and Tuckerman[7] and explore the accessible parameter space. In the following sections, we describe the experimental techniques and present results. It will turn out that Faraday waves can be used to measure interfacial tensions ($\sigma \gtrsim 5 \times 10^{-4}$ N/m). We discuss our surprising finding that measured wavelengths in the ultralow interfacial tension domain are larger by a factor of approximately 2 than the expected values. We hypothesize a key role of the fluid flow associated with the surface waves.

BACKGROUND

Faraday waves are waves excited by vertically oscillating gravity. The interface spawns waves through a parametric instability. In our experiment, the two fluid layers are contained in a closed cell. Its lateral dimension is so large that the sidewalls do not influence the wave pattern, while the layers are so thick that damping of the flow at the top and bottom walls does not influence the onset wavenumber and acceleration amplitude. The absence of boundary effects is a great advantage of this technique for measuring interfacial tension. The insertion of a probe or wavemaker, which could contaminate the interface, is not needed.

For capillary−gravity waves on the interface between two inviscid fluids, the relation between frequency $\omega_0(k)$ and wavenumber k (the dispersion relation) is

$$\omega_0{}^2(k) = \frac{(\rho_1 - \rho_2)gk + \sigma k^3}{\rho_1 + \rho_2} \tag{1}$$

where ρ_1 and ρ_2 are the mass densities of the heavy and lighter fluid, respectively, g is the acceleration of gravity, and σ is the interfacial tension. The derivation of eq 1 assumes irrotational flow, so that the effect of viscous damping is ignored. Via computation of the total dissipation of the potential flow field, a crude approximation of the wavenumber-dependent damping $\gamma(k)$ can be made

$$\gamma(k) = 2\left(\frac{\eta_1 + \eta_2}{\rho_1 + \rho_2}\right)k^2 \tag{2}$$

however, it must be realized that most of the damping arises from the rotational flow near the interface.

Short waves are dominated by the effect of interfacial tension, while long waves are dominated by gravity. In our application, wavenumber k must be large enough such that waves are significantly influenced by interfacial tension. A critical wavenumber follows from equating the terms involving gravity and interfacial tension in eq 1

$$k_\sigma = \left[\frac{g(\rho_1 - \rho_2)}{\sigma}\right]^{1/2} \tag{3}$$

Short waves are increasingly damped. Once the wavenumber becomes larger than k_d, with

$$\omega_0(k_d) = \gamma(k_d) \tag{4}$$

waves are critically damped with the pattern wavelength dominated by damping.

The linear dispersion relation (eq 1) is only approximate. However, it illustrates the finite dynamical range of interfacial tensions that is accessible in experiments using parametric waves. At small interfacial tensions, the pattern wavelength is dominated by the joint effect of gravity and viscous friction, unless the wavenumber is made large. Patterns with large wavenumbers, which are increasingly sensitive to interfacial tension, can be made using high driving frequencies; however, large wavenumbers are more strongly damped, requiring acceleration amplitudes that quickly become unfeasible ($a/g \sim 6$).

In the case of parametric excitation, the elevation amplitude of the interface ζ_k at wavenumber k satisfies the Mathieu equation

$$\ddot{\zeta}_k + \gamma(k)\dot{\zeta}_k + \omega_0{}^2(k)(1 - \tilde{a}\cos\Omega t)\zeta_k = 0 \tag{5}$$

with reduced amplitude

$$\tilde{a} = \frac{\rho_1 - \rho_2}{\rho_1 + \rho_2}\frac{k}{\omega_0(k)^2}a \tag{6}$$

and a the amplitude of the vertical oscillation $a\cos(\Omega t)$. Through the factor $\cos(\Omega t)$, which multiplies the surface elevation $\zeta_k(t)$, higher frequencies with their companion wavenumbers are mixed in. The solution of the resulting coupled equations gives rise to a critical amplitude a_c such that for $a > a_c$ waves with critical wavenumber k_c start to grow.

In the case of infinitely deep fluid layers, the waves that emerge first are the ones where k_c corresponds to waves with a frequency $\Omega/2$ (subharmonic waves).[7] When friction with bottom or top boundaries becomes important, harmonic waves

https://dx.doi.org/10.1021/acs.langmuir.0c00622
Langmuir 2020, 36, 5872−5879

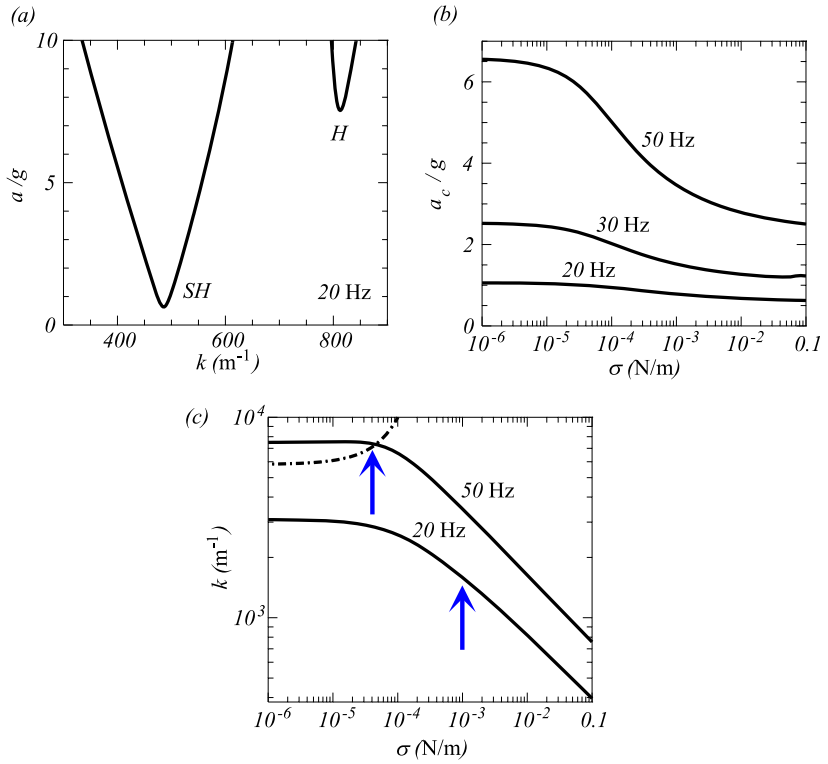

Figure 1. Faraday waves on the interface between water (1) and dodecane (2). The mass densities and viscosities are as follows: $\rho_1 = 1000$ kg m^{-3}, $\rho_2 = 749.5$ kg m^{-3}, $\eta_1 = 1.0 \times 10^{-3}$ kg m^{-1} s^{-1}, and $\eta_2 = 1.34 \times 10^{-3}$ kg m^{-1} s^{-1}. (a) Neutral stability curve for the subharmonic (SH) and harmonic (H) response of an interfacial layer at driving frequency $\Omega = 20$ Hz and interfacial tension $\sigma = 5.287 \times 10^{-2}$ N/m (corresponding to the clean interface). The onset wavenumber k_c and driving amplitude a_c/g where waves first appear on the surface correspond to the minimum of the neutral stability curve. (b) Critical acceleration amplitude a_c/g for Ω values of 20, 30, and 50 Hz. (c) Dependence of the wavenumber k_c of the fastest-growing mode on the interfacial tension σ for driving frequencies Ω of 20 and 50 Hz. For large values of σ, the curves follow the dependence $k \sim \sigma^{-1/3}$ from eq 1. The dashed−dotted line indicates the wavenumber k_d above which waves are critically damped using $\gamma_{k_d} = \omega_{0k_d}$ (eqs 1 and 2). The arrows indicate the wavenumber k_B where gravity and surface tension forces balance, i.e., where the Bond number, $Bo = g(\rho_1 - \rho_2)/(\sigma k_B^2)$, equals 1. At 50 Hz, this occurs when the dependence of k on σ has already flattened due to viscous damping. The results of this figure were computed using the linear Floquet theory of Kumar and Tuckerman.[7]

may emerge first at threshold. Throughout, we assume that the waves selected are not influenced by a quantization condition imposed by the lateral walls of the container. The key parameter is correlation length, which is related to the curvature of the neutral stability curve at $k = k_c$ (see Figure 1a).

The amplitude of the waves is determined by nonlinearity. The linear description predicts unlimited growth for $a > a_c$. Crudely, parametrically excited waves spawn waves with larger wavenumbers through nonlinearities, which, in turn, spawn waves with larger wavenumbers, etc. The proper analysis of weakly nonlinear waves is extremely challenging. A beautiful consequence of nonlinearity is that the threshold amplitude depends on the planar symmetry of the waves. In this way, square, hexagonal, and even quasi-periodic surface wave patterns can be observed at onset.[23−27] Experiments on patterns formed from interfacial waves were reported by Kityk et al.,[28] with results that were reproduced by a direct numerical simulation by Périnet et al.[29]

We have computed neutral stability curves for the fluids used in our experiment using the linear Floquet theory from Kumar and Tuckerman.[7] Briefly, surface deformations are represented by $h(x, t) = \sin(kx) \times \zeta_k(t)$, with $\zeta_k(t)$ expanded in (sub)harmonics of the time-dependent driving force. At each value of interfacial tension σ, we computed the neutral stability curve using 20 Floquet modes.

An example of a neutral stability curve of the subharmonic and harmonic modes that oscillate with frequencies of $\Omega/2$ and Ω, respectively, is shown in Figure 1a. Figure 1b shows the critical amplitude at driving frequencies $\Omega/2\pi$ of 20, 30, and 50 Hz as a function of interfacial tension σ. Due to the small density contrast $\rho_1 - \rho_2$ between the two fluids, the driving is much less efficient than for the single-layer liquid−air system. At small σ values of $\lesssim 10^{-3}$ N/m, large driving amplitudes are needed to excite waves with an increase in driving frequency. These driving amplitudes quickly become unfeasible.

In all of our experiments, we observe a square wave pattern, although our container is circular. Clearly, the symmetry of the wave pattern does not depend on the shape of the container. This independence holds only at excitation amplitudes that are set at a finite distance above onset. Whether the container is so small that the symmetry of the surface wave pattern adapts to that of the sidewalls depends on correlation length ξ. It is defined in terms of the band of wavenumbers Δk that is excited ($\xi = 2\pi/\Delta k$). Because the neutral stability curve is quadratic near onset, $a = a_c + A(k - k_c)^2$, the correlation length is $\xi = \pi A^{1/2}/(a - a_c)^{1/2}$, which diverges at onset. Waves on a very viscous fluid have a small ξ, and their planform is independent of the shape of the container.[30] In the case of Figure 1a, $\xi \approx 70$ cm for excitation amplitudes 10% above onset. This is larger than the size of the container; however, arguments involving ξ

https://dx.doi.org/10.1021/acs.langmuir.0c00622
Langmuir 2020, 36, 5872−5879

assume pinned boundary conditions, which are incompatible with the presence of sidewall meniscii in our experiment.

For very small values of the interfacial tension ($\sigma \lesssim 10^{-4}$ N/m), Figure 1c shows that the pattern wavenumber k_c no longer depends on the interfacial tension. The flattening of the curve $k_c(\sigma)$ is due to the joint effect of gravity and viscous damping. At the density contrast $\Delta\rho = \rho_1 - \rho_2$ of our experiment, the smallest σ that can be detected is determined by gravity. Only for a significantly decreased density contrast does wave damping become the limiting factor. Conversely, for vanishing interfacial tension there is a smallest wavelength λ_{th}, which for small $\Delta\rho$ is determined by viscous damping. Throughout, we will indicate this limiting wavelength. The appearance of a limiting wavelength also poses a limitation on the smallest interfacial tension that can be measured using Faraday waves. The emergence of viscous friction with its influence on the range of measurable σ is owed to the dynamic character of this measurement technique. No such limit exists, in theory, for the pendant drop or the spinning drop technique, which measures the interfacial tension of a static interface.

EXPERIMENTAL SECTION

Our experiment consists of a closed, circular container with an $L = 13$ cm diameter that is mounted on an electromagnetic exciter. The maximum attainable acceleration is approximately 6 g, which limits the smallest wavelength accessible, and thus limits the smallest detectable interfacial tension. The lower part of the container is filled with deionized water (thickness of 1.1 cm), and the upper part (thickness of 0.9 cm) is filled with dodecane. The surfactant (Internal Olefin Sulfonate, Shell Global Solutions International BV) is introduced in the lower water layer, where it is allowed to spread through diffusion over 24 h. Prior to being filled, the container is cleaned with acetone. Next the container is vertically oscillated at frequencies $\Omega/2\pi$ ranging from 10 to 50 Hz. As the driving waveforms were from a frequency synthesizer, the frequency is very accurate. The vertical acceleration of the container was measured with an accelerometer. The interfacial waves were visualized in diffuse lighting, and images were registered stroboscopically at half the driving frequency.

The onset amplitude a_c is determined as the one at which waves first appear after waiting a time τ, τ being on the order of minutes. This measurement of a_c is only approximate; a proper measurement should involve the divergence of τ as $\tau^{-1} \propto (a - a_c)$ when the excitation amplitude approaches a_c. Consequently, our reported onset amplitudes are slightly overestimated.

The wavelength λ of the patterns is determined from Fourier transforming images $I(x, y)$ of the surface, $\tilde{I}(k_x, k_y) = \iint e^{-ik_x x - ik_y y} I(x, y)\, dx\, dy$, averaging $\tilde{I}(k_x, k_y)$ over 300 images, taking an azimuthal average and measuring the location of the first maximum. This procedure is illustrated in Figure 2. In all cases, parametric waves had a square symmetry. As explained in the previous section, this is a consequence of the finite distance of the acceleration amplitude to onset, combined with the soft lateral boundary conditions.

We have also estimated the amplitude of interfacial waves using the method of Moisy et al.,[31] which is designed for the measurement of the topography of a free surface. Figure 3a illustrates its adaptation for interfacial waves. The method is based on the refraction of light at the interface. The refraction depends on the gradient of the interface elevation and is observed through the displacement δ of a dot pattern below the two fluid layers. The displacement field, and thus the interface gradient field ∇h, is measured through spatial correlation of the images of the flat interface and those of the curved interface. Because the contrast of the refractive indices of our two fluids ($n_1 = 1.33$, and $n_2 = 1.42$) is small, the pattern displacements are small, and we can provide elevations only at the lowest driving frequencies.

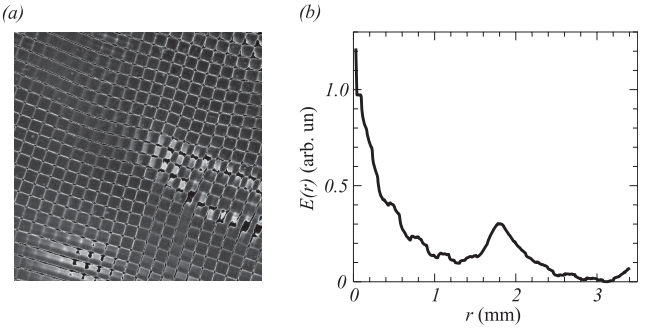

Figure 2. (a) Image of waves at driving frequency $\Omega/2\pi = 50$ Hz and acceleration amplitude $a/g = 4.3$. (b) Azimuthally averaged energy spectrum, indicating a pattern wavelength $\lambda = 1.8$ mm.

We briefly sketch the relation between δ and ∇h, referring to Figure 3a. When the thickness of the glass top and bottom covers is ignored, elementary geometry in the paraxial approximation gives the relationships $n_1\beta = n_2\alpha_2$, $\alpha_3 = \beta - \alpha_2$, $\alpha_4 = n_2\alpha_3$, and $\delta = 2\bar{h}\alpha_4 - h\alpha_3$, leading to the result

$$\delta = (1 - n_1/n_2)\bar{h}(2n_2 - 1)\beta \tag{7}$$

where β is the component of ∇h in the direction of δ, $\bar{h}$ is the average layer thickness, and where we also assume that the pattern is observed from a large height, a condition satisfied in our experiment. Allowing for the relatively thick glass covers of our setup (thicknes d of 4 mm), we obtain

$$\delta = (1 - n_1/n_2)\bar{h}[(2n_2 - 1) + (2n_2 - n_2/n_g)d/\bar{h}]\beta \tag{8}$$

where n_g is the refractive index of the glass covers. From Figure 3c, we conclude that a typical wave amplitude at $\Omega/2\pi = 20$ Hz is ≈0.3 mm. With a wavelength $\lambda \approx 4$ mm, we conclude a wave steepness of ≈0.1. This result will be used for an estimate of the flow-induced surfactant transport in eq 9.

The interaction of surfactant molecules at the interface can be influenced by introducing polar molecules,[32] and in one experiment, NaCl at increasing concentrations was introduced in a mixture of water and 200 ppm surfactant. Upon large additions of salt (≈4 wt % NaCl), we observed the formation of emulsion patches at the interface. The emulsion phase is known to exhibit very small interfacial tensions.[32]

For increasing concentrations Γ, the interfacial tension is expected to drop to ultralow values. A σ reference value of 2.2×10^{-6} N/m was measured for $\Gamma = 200$ ppm using a spinning drop tensiometer.

RESULTS AND DISCUSSION

We have measured the wavelength λ of interfacial waves and the onset excitation amplitude a_c for a clean interface between water and dodecane, and for increasing surfactant concentrations Γ. The excitation frequencies ranged from 20 to 50 Hz. From the measured λ, we have inferred the interfacial tension σ using the Floquet theory of Kumar and Tuckerman.[7] From the measured λ, we can also predict the onset amplitude and compare its value to the one that is actually measured.

Images of the interface for increasing driving frequencies are shown in Figure 4. The wavelength decreases with an increasing frequency Ω; however, all of these wave patterns lead to a consistent estimate of the interfacial tension. The water−dodecane interfacial tension for the clean interface (no surfactant) was measured at four different frequencies, with the result $\sigma = (5.41 \pm 0.05) \times 10^{-2}$ N/m, and no systematic dependence on the frequency. It agrees very well with the literature value of $(5.287 \pm 0.004) \times 10^{-2}$ N/m that was measured by Zeppieri et al.[33] using the pendant drop method.

https://dx.doi.org/10.1021/acs.langmuir.0c00622
Langmuir 2020, 36, 5872−5879

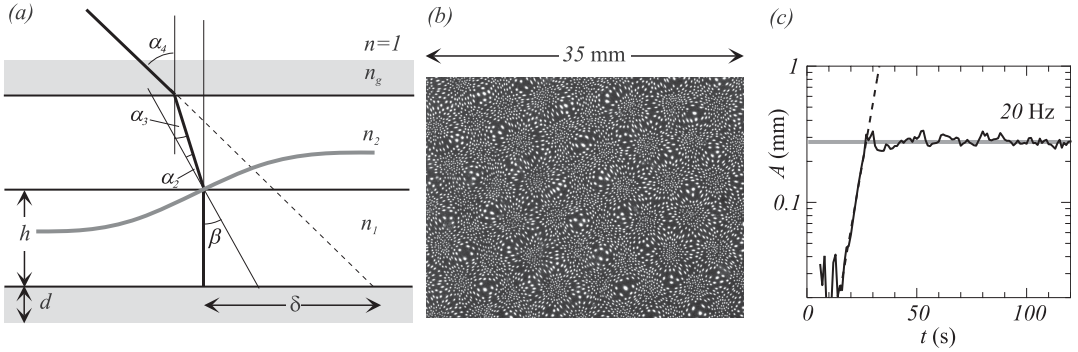

Figure 3. Estimating the amplitude of interfacial waves. (a) The apparent displacement δ of a dot pattern reflects the gradient $\nabla h = \beta$ of the interface. The relation between δ and β follows the derivation by Moisy et al.,[31] but now we also have to account for refraction between the upper fluid layer and air. The refraction at the glass top cover is not shown, but the relation between the gradient ∇h and the apparent displacement δ in eq 9 does allow for these covers. (b) Image of a dot pattern that is deformed by the interfacial waves. (c) Wave amplitude A at driving frequency $\Omega/2\pi = 20$ Hz as a function of time after the start of the excitation. After an exponential rise, the wave amplitude is saturated when $A = 0.3$ mm. It will be used to estimate flow velocities in eq 9.

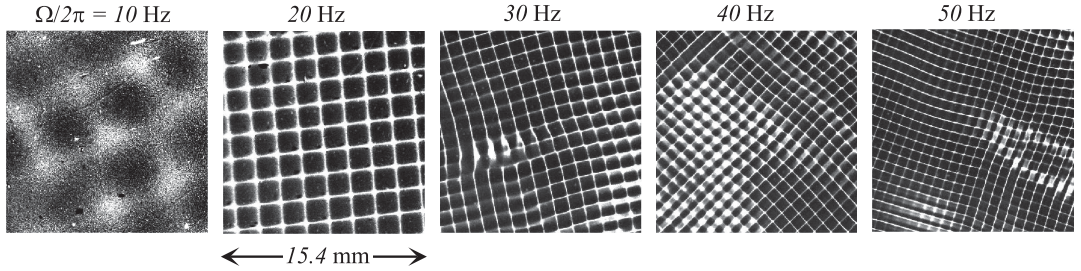

Figure 4. Images of waves at increasing driving frequencies and surfactant concentration $\Gamma = 6$ ppm. For frequencies $\Omega/2\pi > 20$ Hz, the square interface pattern can be recognized clearly.

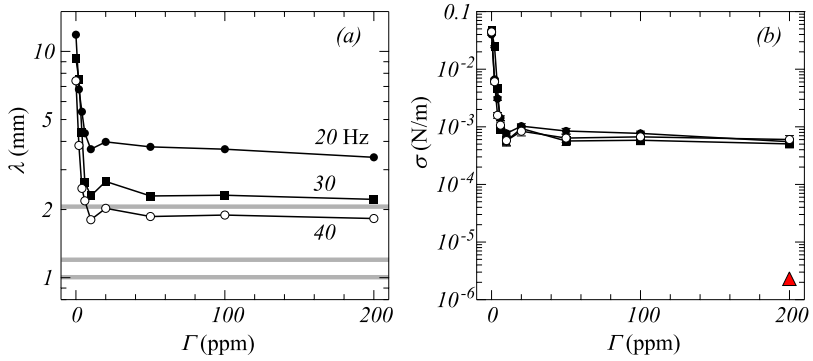

Figure 5. (a) Measured wavelengths of Faraday waves driven at $\Omega/2\pi = 20$, 30, and 40 Hz, for filled circles, filled squares, and empty circles, respectively, as a function of surfactant concentration Γ. The three horizontal lines indicate the minimum wavelength λ_{th} of waves in the limit of vanishing interfacial tension σ. This limiting wavelength decreases monotonically with an increase in frequency. (b) Interfacial tension computed from the wavelengths in panel a. The red triangle indicates a reference measurement of the interfacial tension using a spinning drop tensiometer. The error bars, obscured by the symbols, were computed from the uncertainty in the measured wavelength.

Figure 5a shows the pattern wavelength for three different excitation frequencies as a function of the surfactant concentration. The interfacial tensions, inferred from these wavelengths, are shown in Figure 5b; the results for the three driving frequencies are consistent. The apparent interfacial tension drops steeply when the surfactant concentration is increased to 10 ppm and then stays approximately constant at $\sigma \approx 6 \times 10^{-4}$ N/m. This value is >2 orders of magnitude larger than a reference measurement of σ at $\Gamma = 200$ ppm using a spinning drop tensiometer. The limiting wavelengths λ_{th} are also shown in Figure 5a. In all cases, they are smaller by a factor of 2 than the smallest measured wavelengths.

A series of experiments at $\Gamma = 200$ ppm and varying NaCl concentrations are shown in Figure 6. At the highest NaCl concentrations (≈4%), the formation of patches of a microemulsion was observed on the interface. These patches are free of waves, possibly because of their stronger damping. Wavelengths are measured outside these patches.

The observed wavelengths are larger by a factor of ~2 than the theoretical limiting wavelengths λ_{th} at vanishing interfacial tension. The interfacial tensions computed from these wavelenghts are consistent for the three frequencies.

The consistency of our experiments is further demonstrated in Figure 7 where we compare the measured onset excitation

https://dx.doi.org/10.1021/acs.langmuir.0c00622
Langmuir 2020, 36, 5872−5879

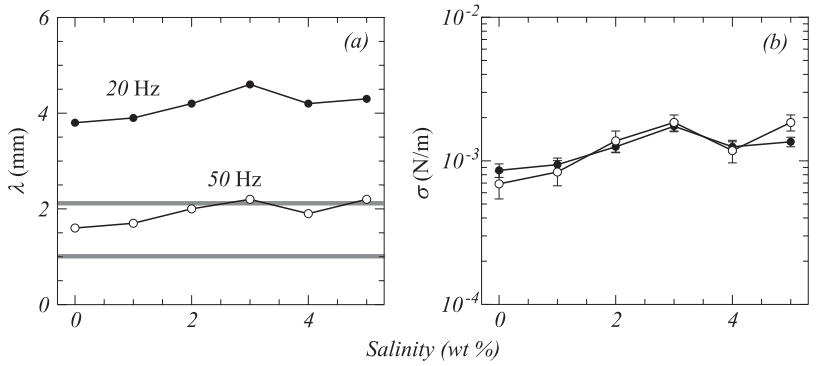

Figure 6. (a) Measured wavelength of Faraday waves driven at $\Omega/2\pi$ = 20 and 50 Hz at a surfactant concentration Γ = 200 ppm and varying salt concentrations. The two horizontal lines indicate the theoretical minimum wavelength λ_{th} of waves in the limit of vanishing interfacial tension σ at driving frequencies of 50 Hz (bottom line) and 20 Hz (top line). (b) Interfacial tension computed from the wavelengths in panel a. The error bars are computed from an uncertainty of 0.2 mm in the measurement of the wavelengths.

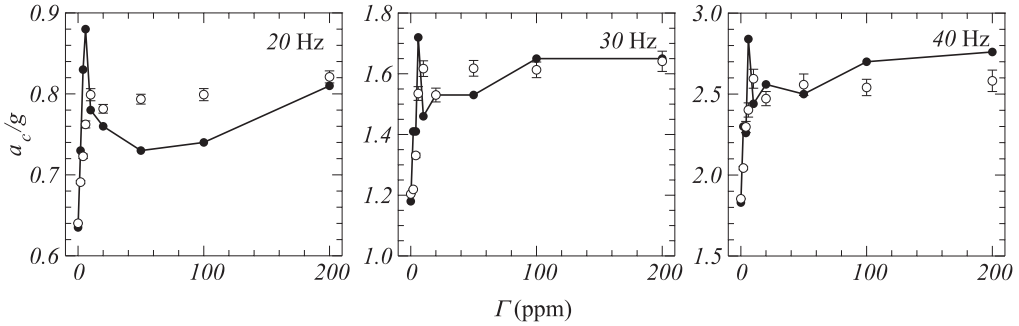

Figure 7. Comparison of computed and measured onset acceleration as a function of surfactant concentration. The computed a_c values were inferred from a measurement of the pattern wavelength, combined with the linear Floquet theory. Filled circles are the direct measurements, and empty circles are computations. The error bars of the computed a_c are derived from the uncertainty in the measured wavelength.

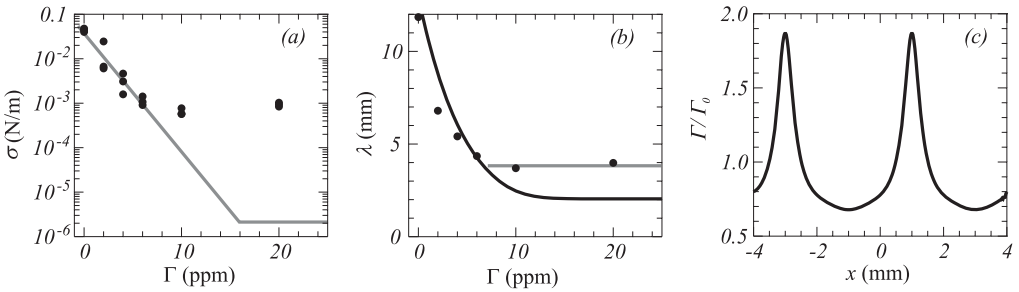

Figure 8. (a) Model equation of state (line), based on our experiments (circles) at low ($\Gamma \lesssim 10$ ppm) and high (Γ = 200 ppm) surfactant concentrations. (b) The black line indicates the wavelength computed from the model EOS in panel a at $\Omega/2\pi$ = 20 Hz; it asymptotes to $\lambda_{th} \approx 2$ mm. The gray line indicates the measured asymptotic wavelength. The circles are the measured wavelengths. (c) Variation of surfactant concentration along the interface due to its bending and stretching. The model velocity field $\mathbf{u}(x, z; t)$ used is for a surface wavelength λ of 4 mm, a driving frequency of 20 Hz, and a wave amplitude of 0.3 mm. The initial concentration is Γ_0.

amplitude a_c with that inferred from the measured pattern wavelength and the Floquet calculation. For surfactant concentrations Γ that are increasing from the clean solvent case Γ = 0 to $\Gamma \approx 6$ ppm, the onset amplitude sharply increases. This is due to the increase in the level of viscous damping as the interfacial tension σ drops and the wavelength decreases. At a surfactant concentration Γ = 200 ppm, the onset amplitudes (a_c/g) corresponding to the static reference measurement of the interfacial tension ($\sigma = 2.2 \times 10^{-6}$ N/m) would have been 1.1, 2.5, and 4.4 for driving frequencies of 20, 30, and 40 Hz, respectively. This is much larger than the measured onset amplitudes.

As a function of increasing surfactant concentration, and thus vanishing interfacial tension, the measured wavelengths and onset accelerations reach asymptotic values. The two measured quantities are perfectly consistent with linear Floquet theory. However, the measured limiting wavelengths are larger by a factor of 2 than the predicted ones, while the observed asymptotic acceleration is much smaller than the prediction.

This striking discrepancy is illustrated in Figure 8. When we assume that the interfacial tension is measured correctly for concentrations $\Gamma \lesssim 10$ ppm, we can draw the crude model equation of state in Figure 8a. The wavelength that follows from this EOS is shown in Figure 8b. At large Γ values, it is smaller by a factor of 2 than the measured wavelength.

There are several ways to escape from this conundrum: either the linear theory fails, or the concentration of surfactant at the interface is much lower than the bulk concentration, and

https://dx.doi.org/10.1021/acs.langmuir.0c00622
Langmuir 2020, 36, 5872−5879

the interfacial tension is much larger than the reference σ measured using the spinning drop technique.

We have no indication that the linear theory fails for interfacial waves. We obtained good agreement with the experiment for the clean interface ($\Gamma = 0$), while the theory has been compared favorably with direct numerical simulations.[29] Also, the predicted onset excitation amplitude agreed with the measured one for all surfactant concentrations.

What we miss is the transport of the surfactant by the flow induced by the waves The surfactant is concentrated at the wave crests and diluted at the troughs. Using our measured wave amplitude, it is possible to crudely estimate the variation of the surfactant concentration $\Gamma(s, t)$ at the interface. It satisfies

$$\Gamma_t + \nabla_s \cdot (\boldsymbol{u}\Gamma) = D_s \nabla_s^2 \Gamma \tag{9}$$

where ∇_s is the gradient along the interface, D_s is the coefficient for diffusion along the interface, and $\mathbf{u}(x, y; t)$ is the fluid velocity field. Approximating $\mathbf{u}(x, z; t)$ with the analytic second-order potential flow solution of Miche[34] (documented by Wright and Saylor[35]), we can easily solve for $\Gamma(s, t)$. The only ingredient needed is a value for the wave amplitude. The influence of diffusion along the surface is negligible because the Peclet number $\mathrm{Pe} = \lambda u_s / D = O(10^2)$.

The variation of Γ for a surface wave amplitude of 0.3 mm (see Figure 3) is shown in Figure 8. The figure illustrates that there is a large variation in Γ over the interface, implying a varying normal stress, and a contribution of tangential stresses (the Marangoni effect). While these concentration variations are relevant around $\Gamma \approx 10$ ppm where the measured wavelength starts to deviate from that predicted, they cannot explain the behavior at ultralow σ. What we still miss is the exchange of the surfactant between the bulk and the interface, the formation of an ultra-low-σ interface in the presence of flow, the surfactant transport in the bulk flow, and, most importantly, the feedback of the interfacial tension modulation on the flow.

CONCLUSION

Interfacial tensions can be measured using Faraday waves. The measurement is quick, is insensitive to boundaries, and needs only analysis of images. However, the dynamic range of σ is limited from below to $\gtrsim 5 \times 10^{-4}$ N/m. At very small interfacial tensions, we hypothesize the influence of surfactant dynamics that causes larger effective interfacial tensions than what is expected on the basis of the bulk surfactant concentration.

AUTHOR INFORMATION

Corresponding Author

Willem van de Water − *Laboratory for Aero and Hydrodynamics, Delft University of Technology and J. M. Burgers Centre for Fluid Dynamics, 2628 CD Delft, The Netherlands;* orcid.org/0000-0002-1054-9780; Email: w.vandewater@tudelft.nl

Authors

Yuk Man Lau − *Laboratory for Aero and Hydrodynamics, Delft University of Technology and J. M. Burgers Centre for Fluid Dynamics, 2628 CD Delft, The Netherlands*

Jerry Westerweel − *Laboratory for Aero and Hydrodynamics, Delft University of Technology and J. M. Burgers Centre for Fluid Dynamics, 2628 CD Delft, The Netherlands*

Complete contact information is available at: https://pubs.acs.org/10.1021/acs.langmuir.0c00622

Notes

The authors declare no competing financial interest.

ACKNOWLEDGMENTS

This research was supported by Shell Technology Centre Amsterdam (STCA), The Netherlands and Shell Global Solutions International B.V., The Netherlands (Grant PT66562). The authors thank Mark Brewer for the fluid samples and gratefully acknowledge many helpful discussions with Damir Juric and Laurette Tuckerman.

REFERENCES

(1) Cabezas, M. G.; Bateni, A.; Montanero, J. M.; Neumann, A. W. Determination of Surface Tension and Contact Angle from the Shapes of Axisymmetric Fluid Interfaces without use of Apex Coordinates. *Langmuir* **2006**, *22*, 10053−10060.

(2) Vonnegut, B. Rotating bubble method for the determination of surface and interfacial tensions. *Rev. Sci. Instrum.* **1942**, *13*, 6−9.

(3) Seiffert, A. In *Drops and bubbles in interfacial research*; Möbius, D., Miller, R., Eds.; Elsevier, 1989; pp 187−238.

(4) Bolognesi, G.; Saito, Y.; Tyler, A. I. I.; Ward, A. D.; Bain, C. D.; Ces, O. Mechanical characterization of ultralow interfacial tension oil-in-water droplets by thermal capillary wave analysis in a microfluidic device. *Langmuir* **2016**, *32*, 3580−3586.

(5) Muijlwijk, K.; Hinderink, E.; Ershov, D.; Berton-Carabin, C.; Schroën, K. Interfacial tension measured at high expansion rates and within milliseconds using microfluidics. *J. Colloid Interface Sci.* **2016**, *470*, 71−79.

(6) Moiré, M.; Peysson, Y.; Herzhaft, B.; Pannacci, N.; Gallaire, F.; Augello, L.; Dalmazzone, C.; Colin, A. Ultralow interfacial tension measurement through jetting/dripping transition. *Langmuir* **2017**, *33*, 2531−2540.

(7) Kumar, K.; Tuckerman, L. Parametric instability of the interface between two fluids. *J. Fluid Mech.* **1994**, *279*, 49−68.

(8) Mandelstam, L. Über die Rauhigkeit freier Flüssigkeitsoberflächen. *Ann. Phys.* **1913**, *346*, 609−624.

(9) Aarts, D.; Schmidt, M.; Lekkerkerker, H. Direct Visual Observation of Thermal Capillary Waves. *Science* **2004**, *304*, 847.

(10) Zhou, H.; Gabilondo, B. B.; Losert, W.; van de Water, W. Stretching and relaxation of vesicles. *Phys. Rev. E* **2011**, *83*, 011905.

(11) Lucassen-Reynders, E. H.; Lucassen, J. Properties of capillary waves. *Adv. Colloid Interface Sci.* **1970**, *2*, 347−395.

(12) Saylor, J. R.; Szeri, A. J.; Foulks, G. P. Measurement of surfactant properties using a circular capillary wave field. *Exp. Fluids* **2000**, *29*, 509−518.

(13) Strickland, S. L.; Shearer, M.; Daniels, K. E. Spatiotemporal measurement of surfactant distribution on gravity-capillary waves. *J. Fluid Mech.* **2015**, *777*, 523−543.

(14) Fauve, S.; Kumar, K.; Laroche, C.; Beysens, D.; Garrabos, Y. Parametric instability of a liquid-vapour interface close to the critical point. *Phys. Rev. Lett.* **1992**, *68*, 3160−3.

(15) Huber, P.; Soprunyuk, V. P.; Embs, J. P.; Wagner, C.; Deutsch, M.; Kumar, S. Faraday instability in a surface-frozen liquid. *Phys. Rev. Lett.* **2005**, *94*, 184504.

(16) Henderson, D. Effects of surfactants on Faraday-wave dynamics. *J. Fluid Mech.* **1998**, *365*, 89−107.

(17) Kumar, S.; Matar, O. K. On the Faraday instability in a surfactant-covered liquid. *Phys. Fluids* **2004**, *16*, 39−46.

(18) Kumar, S.; Matar, O. K. Instability of long-wavelength disturbances on gravity-modulated surfactant-covered thin liquid layers. *J. Fluid Mech.* **2002**, *466*, 249−258.

(19) Suman, B.; Kumar, S. Surfactant- and elasticity-induced inertialess instabilities in vertically vibrated liquids. *J. Fluid Mech.* **2008**, *610*, 407−423.

(20) Matar, O. K.; Kumar, S.; Craster, R. V. Nonlinear parametrically excited surface waves in surfactant-covered thin liquid films. *J. Fluid Mech.* **1999**, *520*, 243−265.
(21) Shin, S.; Chergui, J.; Juric, D.; Kahouadji, L.; Matar, O. K.; Craster, R. V. A hybrid interface tracking-level set technique for multiphse flow with soluble surfactant. *J. Comput. Phys.* **2018**, *359*, 409−435.
(22) Ubal, S.; Giavedoni, M. D.; Saita, F. A. Elastic effects of an insoluble surfactant on the onset of two-dimensional Faraday waves: a numerical experiment. *J. Fluid Mech.* **1999**, *524*, 305−329.
(23) Chen, P.; Viñals, J. Pattern selection in Faraday waves. *Phys. Rev. Lett.* **1997**, *79*, 2670−2673.
(24) Chen, P.; Viñals, J. Amplitude equations and pattern selection in Faraday waves. *Phys. Rev. E* **1999**, *60*, 559−70.
(25) Binks, D.; van de Water, W. Nonlinear pattern formation of Faraday waves. *Phys. Rev. Lett.* **1997**, *78*, 4043−6.
(26) Binks, D.; Westra, M.; van de Water, W. Effect of depth on the pattern formation of Faraday waves. *Phys. Rev. Lett.* **1997**, *79*, 5010−3.
(27) Westra, M.; Binks, D. J.; van de Water, W. Patterns of Faraday waves. *J. Fluid Mech.* **2003**, *496*, 1−32.
(28) Kityk, A. V.; Embs, J.; Mekhonoshin, V. V.; Wagner, C. Spatiotemporal characterization of interfacial Faraday waves by means of light absorption technique. *Phys. Rev. E* **2005**, *72*, 036209.
(29) Périnet, N.; Juric, D.; Tuckerman, L. S. Numerical simulation of Faraday waves. *J. Fluid Mech.* **2009**, *635*, 1−26.
(30) Edwards, W.; Fauve, S. Patterns and quasi-patterns in the Faraday experiment. *J. Fluid Mech.* **1994**, *278*, 123−48.
(31) Moisy, F.; Rabaud, M.; Salsac, K. A synthetic Schlieren method for the measurement of the topography of a surface. *Exp. Fluids* **2009**, *46*, 1021−1036.
(32) Unsal, E.; Broens, M.; Armstrong, R. T. Pore dynamics of microemulsion formation. *Langmuir* **2016**, *32*, 7096−7108.
(33) Zeppieri, S.; Rodríguez, J.; López de Ramos, A. L. Interfacial tension of Alkane + Water systems. *J. Chem. Eng. Data* **2001**, *46*, 1086−1088.
(34) Miche, M. Mouvements ondulatoires de la mer en profondeur constante ou d'écroissante. *Ann. Ponts Chaussees* **1944**, *144*, 25.
(35) Wright, P. H.; Saylor, J. R. Patterning of particulate films using Faraday waves. *Rev. Sci. Instrum.* **2003**, *74*, 4063.

https://dx.doi.org/10.1021/acs.langmuir.0c00622
Langmuir 2020, 36, 5872−5879